JGR Atmospheres

RESEARCH ARTICLE
10.1029/2024JD042739

Hurricane Hilary (2023) and Rare Tropical Cyclones in the Southwest United States: Impacts on Temperature and Precipitation

Euan Miles[1] **and Shang-Ping Xie**[1]

[1]Scripps Institution of Oceanography, University of California, San Diego, CA, USA

Key Points:

- Rare tropical cyclones (TCs), such as Hurricane Hilary in 2023, bring extreme rainfall and modulate local temperatures in the Southwest US
- Composite analysis of 42 TCs shows that coastal temperatures warm significantly as TCs approach
- This warming is driven by downslope winds, suppression of coastal upwelling, and temperature advection

Supporting Information:

Supporting Information may be found in the online version of this article.

Correspondence to:

E. Miles,
edmiles@ucsd.edu

Citation:

Miles, E., & Xie, S.-P. (2025). Hurricane Hilary (2023) and rare tropical cyclones in the Southwest United States: Impacts on temperature and precipitation. *Journal of Geophysical Research: Atmospheres*, *130*, e2024JD042739. https://doi.org/10.1029/2024JD042739

Received 15 NOV 2024
Accepted 4 FEB 2025

Abstract Hurricane Hilary brought extensive, record-breaking precipitation to the Southwest United States in August 2023. Although tropical cyclones (TCs) are uncommon in this region, they can cause substantial damage, primarily through flooding. However, heat extremes associated with these TCs are understudied and could have significant impacts in populated coastal areas. This study examines the conditions that promoted the occurrence of 42 north-reaching, northeastern Pacific TCs and quantifies how local temperatures responded to these storms. Using composite analysis, we find that there is significant warming along the coastal region of Southern California preceding a TC, particularly for storms that remain offshore. Three main mechanisms contribute to this warming pattern—adiabatic compression associated with downslope winds, warm air advection by the TC itself, and suppression of coastal upwelling. These compound heatwave-TC events are an overlooked impact of TCs that will likely become more important as the climate warms.

Plain Language Summary Hurricane Hilary caused record-breaking rainfall across the Southwest United States in August 2023. Tropical cyclones (TCs) that affect this region are rare but have caused damage from flooding in the past. Another, understudied, aspect of these storms is their impact on local temperatures. In this study, we examine the conditions that cause TCs to travel toward the Southwest US and describe how they influence temperatures in the region. We average the conditions associated with 42 TCs and find that there is significant warming in coastal Southern California as these storms approach. This warming is caused by three factors—winds flowing down the mountains toward the coast, winds bringing warm air from the south, and warming of sea-surface temperatures near coast. This highlights how, as well as bringing damaging wind and rain, TCs can cause extreme heat. This risk is likely to increase as climate change causes global temperatures to rise.

1. Introduction

In August 2023, Hurricane Hilary brought significant and extensive rainfall to the Southwest United States (SW US). Downtown San Diego and Los Angeles both set August daily rainfall records (Cassidy, 2023) and there was widespread flash flooding, debris flows, and power outages in Baja California and Southern California. The storm was well-forecasted, and the National Hurricane Center (NHC) issued its first ever tropical storm warning for California (National Hurricane Center, 2023). Although recent analysis shows that convection became disorganized over northern Baja California and that Hilary did not reach California as a TC as originally thought (Steen et al., 2023), the event still caused at least three deaths and $900 million of damage in the US (Reinhart, 2024), raising questions about the risk that TCs and their remnants pose to this region.

Hilary was an exceptional event for Southern California but was not without precedent. During the 20th century, four storms have brought tropical storm-force winds to the SW US—Nora in 1997, Kathleen in 1976, Joanne in 1972, and a storm in 1939 which made direct landfall in Southern California. The only known system to bring hurricane-force winds to California was the San Diego Hurricane of 1858 (Chenoweth & Landsea, 2004). These events all caused substantial damage—70% of Ocotillo was destroyed during flash flooding during Kathleen (Fors, 1977), at least 45 people were killed during the 1939 storm (Blake et al., 2007), and millions of dollars of loss were associated with Nora (Lawrence, 1999).

TCs can still impact the SW US without directly hitting the region, with such a system typically occurring every year or two (Smith, 1986). Corbosiero et al. (2009) found 35 TCs that brought significant precipitation to the region between 1958 and 2003, and Ritchie et al. (2011) investigated 43 TC remnants that impacted the SW US

from 1992 to 2005. These systems are generally associated with deeper than normal offshore troughs and anomalous anticyclonic conditions over the continent, which steers TCs to the north, rather than to the east (Corbosiero et al., 2009). However, they tend to weaken very quickly due to high vertical shear and low sea-surface temperatures (SSTs), meaning that the main impact of TCs and their remnants to the SW US is from extreme precipitation rather than wind (Ritchie et al., 2011). Gulf moisture surges associated with the passage of a TC near the southern tip of Baja California can also bring significant rainfall to the monsoon region even if the system does not track over the SW US (Higgins & Shi, 2005; Rogers & Johnson, 2007).

In addition to extreme rainfall, TCs can significantly modulate the air temperature of regions they pass over. Over southeastern China, P. Wang et al. (2023) found that TCs can increase local temperatures by enhancing anticyclonic circulation patterns. Increased attention is being given to these compound TC-heatwave events due to their potential to amplify impacts, particularly in the event of power outages and failure of air conditioning systems (K. Feng et al., 2022). In the SW US, unlike most places impacted by TCs, temperatures and TC likelihood peak at roughly the same time of year (Matthews et al., 2019; Ritchie et al., 2011). Record-breaking heat in California—associated with 395 excess deaths in the state—occurred prior to the passage of TC Kay in September 2022, with temperatures cooling significantly in its aftermath (Milet et al., 2023; Pratt, 2022).

Previous work has investigated the contribution of TCs to precipitation in the SW US, but their impact on temperatures in the region has not been quantified (Corbosiero et al., 2009; Ritchie et al., 2011). Here, temperature anomalies and rainfall associated with 42 TCs that affected the SW US between 1959 and 2023 are considered. In general, we find that there is significant warming in the highly populated coastal region of Southern California preceding a TC, particularly when a TC passes just offshore. We also give special attention to the recent Hurricane Hilary and the conditions that brought such extreme precipitation to the SW US.

2. Data and Methods

Eastern and Central Pacific TC tracks from 1959 to 2023 were taken from the NHC Best Track Data Set (HURDAT2, Landsea & Franklin, 2013). TCs are typically tracked every 6 hr by the NHC, so six-hourly ERA5 reanalysis data from the European Centre for Medium-Range Weather Forecasts (ECMWF, Hersbach et al., 2020) was used to assess the large-scale meteorological fields at the time of TC passage. Precipitation data are hourly. Anomalies are calculated from an 11-day running-mean climatology.

Forty-two TCs that reached a latitude of at least 29°N between 1959 and 2023 were split into two groups for composite analysis—those that passed 29°N between 125° and 115°W—the western group—and those that passed between 115°W and 105°W—the eastern group (Tables S1 and S2 in Supporting Information S1). Corbosiero et al. (2009) and Ritchie et al. (2011) also split TCs into groups but used subjective rainfall patterns associated with each TC rather than position at their northern extremity to divide the storms. TCs can also be grouped by their track using a probabilistic cluster analysis technique developed by Gaffney (2004; see also Camargo et al. (2007)). We opted for the simpler east-west grouping as this allowed for a clear physical interpretation.

To investigate the temperature and precipitation response to TCs in each group, we made area-averaged timeseries composites over coastal and inland regions of the SW US. The coastal region consists of all near-coast grid cells with an elevation below 750 m between 31° and 36°N, including Los Angeles, San Diego, and Tijuana. The inland region extends from the eastern edge of the peninsular ranges to 111°W, bounded by 29°N and 34°N. Twenty-four-hour running means were taken to remove any diurnal variations. Anomalies were considered significant when they exceeded the 95% confidence level of a one-tailed students' *t*-test (Student, 1908).

To ensure conclusions are robust, observational temperature data from National Weather Service (NWS) stations was compared with gridded ERA5 reanalysis. Daily mean temperature anomaly data (with anomalies from the 1991–2020 mean) for the South Coast Drainage Basin region of California was taken from the US Climate Resilience Toolkit's SC-ACIS (U.S. Climate Resilience Toolkit, 2024). We used SC-ACIS data for the local date that a TC crosses 29°N and compared it to ERA5 data, which occurs on the same local day (the average of four timesteps at 12, 18, 00, and 06 UTC). For this analysis only, ERA5 data were normalized using the period 1991–2020 to allow for direct comparison between reanalysis and observations. Average observational temperature

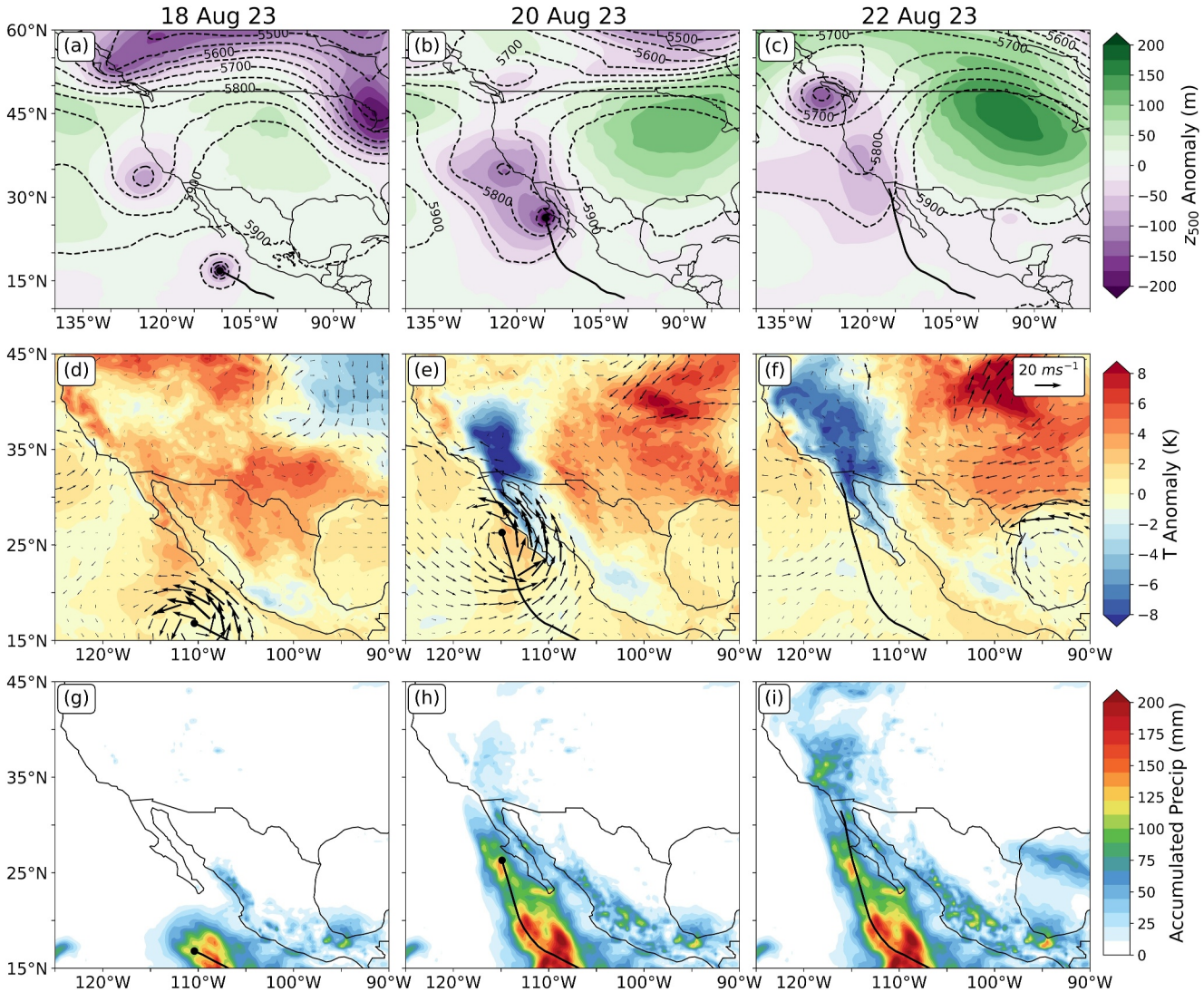

Figure 1. Meteorological snapshots during tropical cyclone (TC) Hilary's track toward Southern California in August 2023. (a)–(c) 500 hPa geopotential height anomalies at 12 UTC on the dates show. (d)–(f) 24-hr-averaged 2 m temperature anomalies and 850 hPa wind anomalies for the dates shown. (g)–(h) 3-day, 5-day, and 7-day precipitation accumulation totals respectively, ending at 12UTC on the date shown. The black lines in each plot show the track of TC Hilary, with the black dots the storm's position at 12UTC on the date shown.

anomalies during TC occurrence were overlaid on a composite of gridded ERA5 data, with an individual station shown if there are measurements during at least 70% of the TCs. A full list of stations used is shown in Table S3 in Supporting Information S1.

3. Results

3.1. Hurricane Hilary

Tropical Storm Hilary formed on 16 August 2023, and rapidly intensified into a category 4 hurricane in the presence of warm SSTs and weak vertical shear. The development of a deep trough over the Pacific and strong anticyclone over the central US then steered the storm toward the north, where it made landfall on the northwest coast of Baja California. The top row of Figure 1 shows that both the trough and ridge strengthened between August 18 and 20, and caused Hilary to accelerate to the north, moving with a faster maximum translational speed than any other TC considered in this analysis. Hilary lost its tropical characteristics in northern Baja California with a separate, non-tropical, area of low pressure forming near San Diego and absorbing its remnants by August

21. However, there were still significant impacts in Southern California—a peak wind gust of 140 kmph was recorded at Magic Mountain in LA County, and a maximum total rainfall of 332 mm occurred on the eastern edge of the San Bernadino mountains. See the NHC TC report for further details on Hilary's synoptic history and impacts (Reinhart, 2024).

Temperatures in the SW US were broadly 1–4°C higher than average on August 18 but Hilary's approach induced a rapid cooling, with anomalies up to −10°C across inland Southern California, Nevada, and Arizona (Figure 1e). This cooling was driven first by increased cloud cover (Figure S1 in Supporting Information S1) and then the intense rainfall associated with the storm. There was a much smaller temperature response on the coast, and the hot temperature anomalies in the central and eastern US were driven by a strong anticyclone (Doermann, 2023). The bottom row of Figure 1 shows the progression of precipitation accumulation for the week ending on August 22 (most of the rain in the US and Baja California being associated with Hilary and the post-tropical low that absorbed its remnants). Rainfall follows the track of the TC closely which is the heaviest offshore of Mexico and on the slopes of the mountain ranges of Southern California. This precipitation pattern could be considered an extreme case of the "California-Nevada track" in Corbosiero et al. (2009) or the "north/northwest movement" group in Ritchie et al. (2011). Hilary was well-predicted by models, with ample time for preparations to be made in Southern California (Reinhart, 2024); however, a small change to the track could have had a large influence on the impacts of the storm. Farfán and Zehnder (2001) found that the peninsular mountain ranges of Baja California, over which Hilary dissipated, were critical to altering the convective structures of Hurricane Nora in 1997. Significantly stronger winds would have been likely had the TC stayed offshore for longer, allowing the windier right side of the storm (Du et al., 2023) to pass over populated regions in coastal Southern California, as was the case in the hurricane of 1858 (Chenoweth & Landsea, 2004). Although Hilary was a rare event, it did not represent the worst-case scenario for the region.

3.2. North-Reaching TCs

The TC season in the NEP runs from May 15th to November 30th, with the peak season occurring at the end of July (Corbosiero et al., 2009; Landsea & Franklin, 2013). However, TCs reaching 29°N occur almost exclusively in the mid-to-late season, with over 60% occurring in September. Around 10% of all September NEP TCs reach 29°N compared to a seasonal average of 3.7%. Figure 2 shows the occurrence of north-reaching TCs in the NEP along with the climatology of SSTs, wind shear, and mean sea-level pressure. Warmer SSTs, weaker climatological shear, and a deeper mid-level trough protruding further to the south occur in September and produce far more favorable conditions for these TCs. A strong trough off the west coast of the US can steer TCs quickly to the north, meaning that they spend limited time over unfavorable SSTs, with lower climatological shear also reducing the rate at which they weaken (Gray, 1968).

There are also various modes of variability that influence TC tracks and frequency. El Niño is thought to aid the formation of TCs in the NEP; however, it also shifts the main region of activity west, reducing near-coastal TC counts (Lin et al., 2020). We found a statistically significant above-averaged Niño3.4 index (calculated using ERA5 SST data, Hanley et al., 2003) of 0.468 during TC occurrence at 29°N, and noted that north-reaching TCs seem to occur preferentially during the strongest El Niño years. Previous research has also linked other modes of variability such as the Pacific Meridional Mode and Pacific Decadal Mode (Gutzler et al., 2013; Murakami et al., 2017), as well as upper ocean heat content and North Atlantic conditions (Caron et al., 2015) to TC counts in the eastern Pacific; however, we do not quantify their influence here due to the small sample size in our analysis.

The top row of Figure 3 shows the tracks of all the TCs considered in this study, split into "western" and "eastern" groups. The 24 TCs in the western group tend to follow the coast of Baja California and approach Southern California with primarily northward motion. The 18 TCs in the eastern group generally recurve to the east, crossing over Baja California and into Arizona. There is a distinct trough off the west coast and a ridge over the continent for both groups (Figures 3c and 3d), with a deeper trough located further to the east for TCs that recurve to the northeast. The offshore trough is a very robust feature, present in almost all the TC analyzed.

3.3. Temperature and Precipitation Response to TCs

The temperature and precipitation responses associated with TCs in each group are shown in the composites in the bottom two rows of Figure 3. As TCs in the western group approach Southern California, there is strong anomalous warming along the coast, with weak cooling on the eastern side of the peninsular mountain ranges.

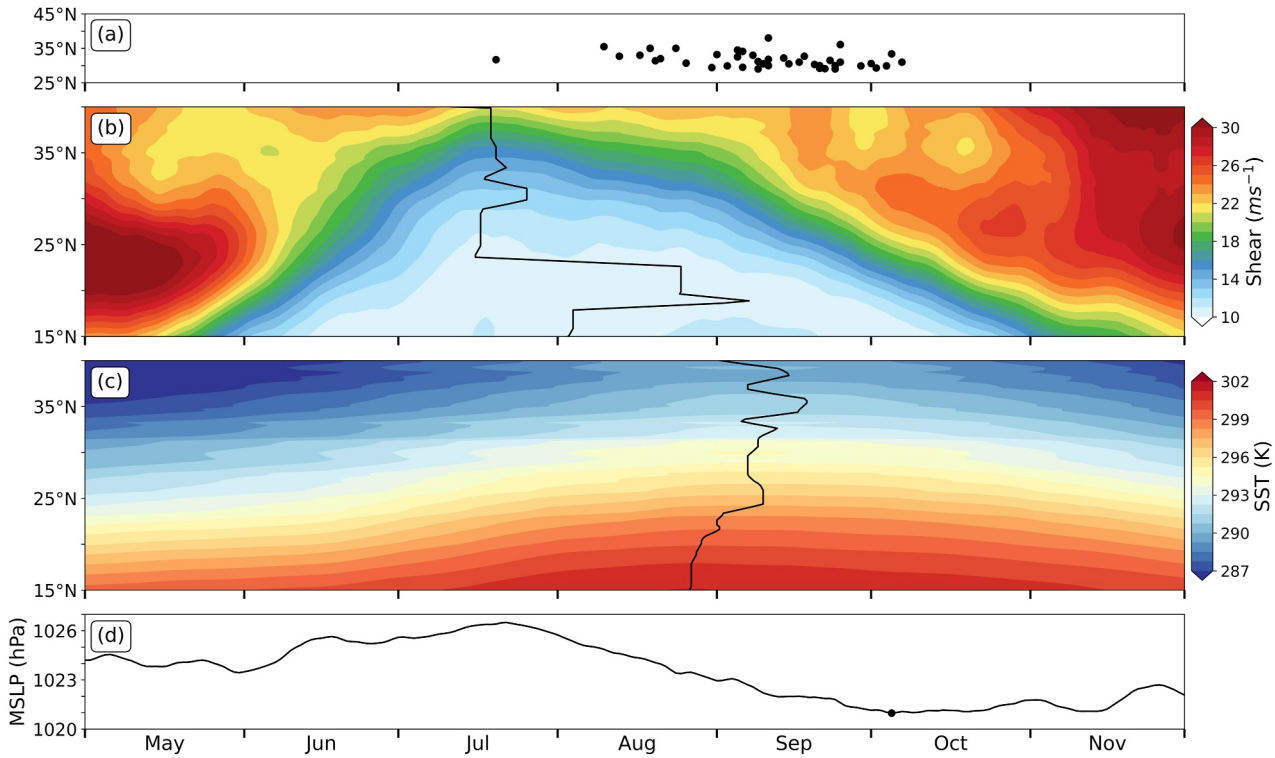

Figure 2. Climatology of tropical cyclone (TC) counts reaching 29°N and factors influencing their tracks. (a) The 42 TCs in the analysis shown by their maximum latitude and the date that they reached 29°N. (b) Hovmöller of climatological vertical wind shear (difference between wind speed at 200 hPa and 850 hPa), averaged at each latitude between 130° and 105°W, with the black line showing the date of minimum wind shear at each latitude. (c) Hovmöller of climatological sea-surface temperatures (SSTs) averaged between 130° and 105°W, with the black line showing the date of maximum SST at each latitude. (d) Strength of the subtropical North Pacific High, measured by the maximum MSLP in the area bounded by 20°S, 50°N, 160°W, and 120°W, with the black dot showing the date of the minimum strength.

When TCs instead track toward northern Mexico and Arizona, there is a much stronger inland cooling signal and weaker coastal warming response. For TCs in the western group, precipitation is dispersed, with much of it occurring over the ocean; however, the composite shows accumulation of about 20–30 mm on the San Bernadino and Sierra Nevada mountains. On the other hand, TCs in the eastern group bring almost no rainfall to the west coast of California, but significant accumulations occur in the inland desert regions of Arizona and northern Mexico, and along the coastal regions on either side of the Gulf of California.

Figure 4 shows the time-evolution of temperature in defined coastal and inland regions for each TC group. In the coastal region, there is a sharp warm temperature response to western group TCs (Figure 4a), peaking at about 2°C above normal, before temperatures fall when rainfall begins. We identify three key mechanisms which drive this warming. First, southerly wind anomalies associated with the cyclonic circulation of offshore storms suppress coastal upwelling (Huyer, 1983; Wei et al., 2021), gradually causing near-coast SSTs to warm (bottom row of Figure S2 in Supporting Information S1). However, surface air temperature anomalies extend far offshore (Figure 3e) and are substantially higher than SST anomalies, suggesting that this is not the only cause. Advection of warm air from the south due to the strong TC winds drives the broad area of warming that extends out from the coast. Temperature anomalies of up to 2°C are seen to the northeast of TCs in composites of offshore TCs in the NEP (Figure S4 in Supporting Information S1), and this feature is identified in many of the TCs in this analysis as they track along the coast of Baja California.

Third, there is also an easterly wind component associated with approaching TCs, which flows across the peninsular ranges of Baja California and Southern California, causing near-surface warming due to adiabatic compression from downslope winds. The top row of Figure 5 shows the evolution of coastal warming during western group TCs, with a vertical transect across the mountains of Southern California showing downward vertical wind anomalies and associated warming. Both easterly and downward winds peak as the TCs reach 29°N, and this is associated with a temperature anomaly of over 4°C, largest at the 975 hPa level. As a TC

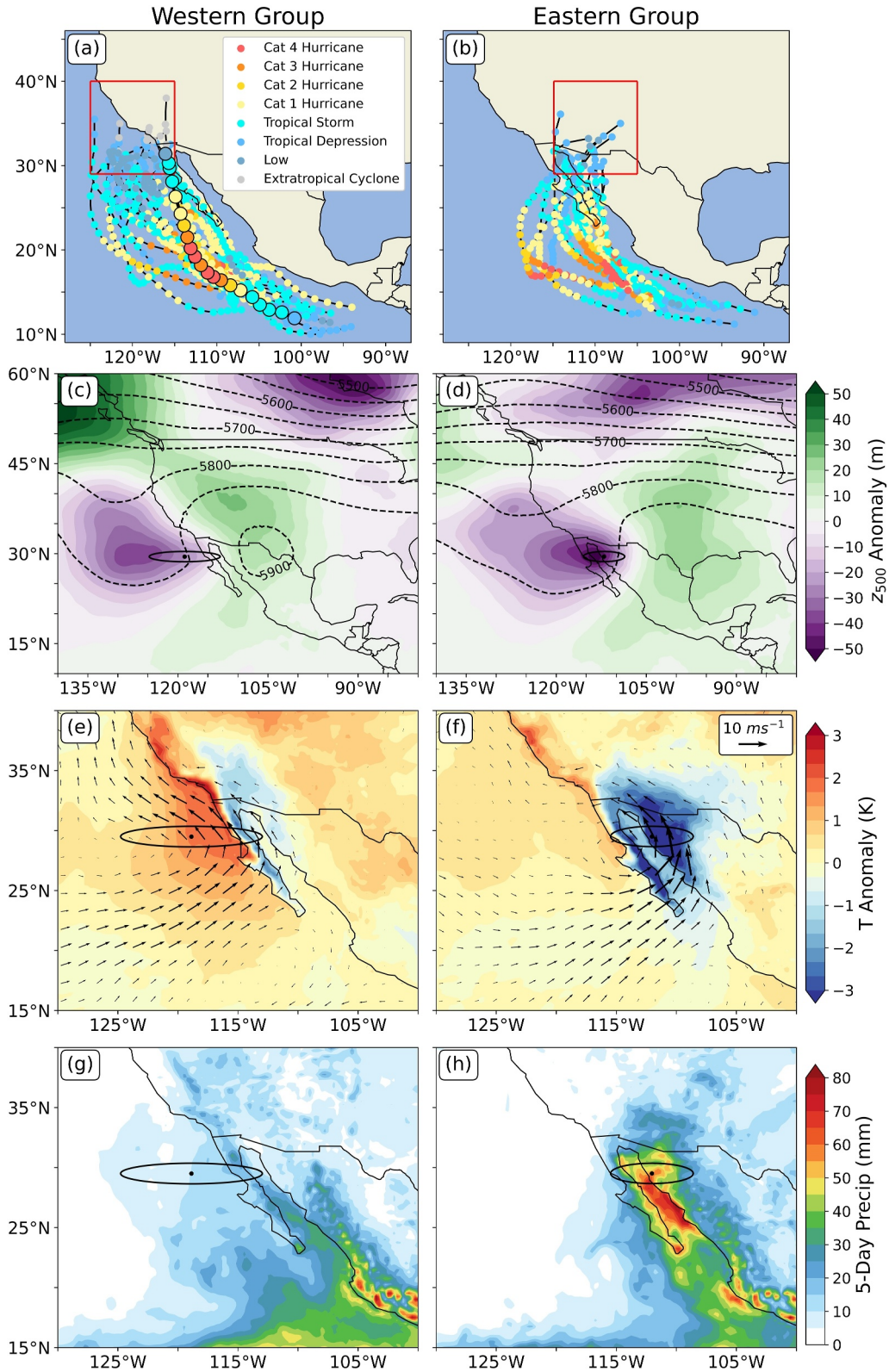

Figure 3.

passes to the north or dissipates, easterly winds subside, downward winds are no longer present, and positive temperature anomalies weaken significantly. This process is clear when looking at individual TCs, particularly Lidia in 2017 and Claudia in 1962, both of which feature strong wind anomalies from the northeast, that brought warm temperatures to the populated coastal areas of Southern California. The effects of downslope winds are also visible during eastern group TCs, albeit producing a much weaker coastal temperature response (bottom row of Figure 5). It is worth noting that this pattern of coastal warming is very similar to that of a warm Santa Ana wind event, which features strong northeasterly winds from the Great Basin driving adiabatic compression (Gershunov et al., 2021). In the inland region, around a week before a TC in the eastern group reaches 29°N, there is also a period of statistically significant warm temperatures. Temperatures persist around 1.5°C above average for a week before the storm brings precipitation and cooler temperatures. This is associated with a strong positive 500 hPa geopotential height anomaly, which is visible over the western half of the US in a composite of TCs in the eastern group. We do not establish a clear link between this ridge feature and the TCs themselves, but it is possible that a general eastward propagation of continent-scale circulation patterns makes the occurrence of a ridge prior to the trough seen in Figure 3d a consistent feature that brings warm temperatures before many of the eastern group TCs. Furthermore, ridge-building can be associated with recurvature (visible in Figure 3b for many of the eastern group TCs) and extratropical transition (Evans et al., 2017). Although we see the strong downstream signal in both 500 hPa geopotential height and temperature prior to the recurvature of these TCs, this mechanism may help to prolong the ridge feature over the central US as seen in Figures S3c and S3d in Supporting Information S1.

For both groups and regions, there is a significant cooling trend once TCs reach 29°N. This is particularly prominent for eastern group TCs, where the mean temperature anomaly in the inland region falls by over 4°C and precipitation peaks at over 0.6 mm per hour as a TC passes (Figure 4d). The negative temperature anomaly is driven by evaporative cooling, with Figure S5 in Supporting Information S1 showing a peak in latent heat loss by the surface during this cooling. There is also a decrease in surface insolation as the TC brings increased cloud cover (Figures S3 and S5 in Supporting Information S1), further cooling the region. On average, it takes around 5 days before temperatures return to normal in the inland region following a TC event. The response to western group TCs is weaker, as they tend to be associated with much less precipitation over the inland region, though Hilary in 2023 and Kathleen in 1976 were notable exceptions to this.

The evolution of these temperature responses across a transect at 33°N are visualized in the Hovmöller diagrams in Figure 6. From Figure 6a, we see that near-coast warming peaks when the TC is slightly to the south, when easterly, cross-mountain, flow is maximal. A second temperature peak further offshore is likely related to the advection of warm air from the south, occurring to the northeast of the TC. Coastal land temperatures drop quickly as downslope winds cease and precipitation drives evaporative cooling. The coastal temperature response to eastern group TCs is about half the magnitude as for the western group (Figure 6b), but weak easterly wind anomalies also drive some surface coastal warming. Air temperature anomalies over the ocean remain positive due to persisting above-average SSTs, particularly for western group TCs, where stronger southeasterly winds effectively suppress coastal upwelling. Rainfall rates are significantly higher during eastern group TCs, and subsequent cooling is significantly larger. Both rainfall and the main region of cooling are shifted much further east during these TCs.

3.4. Comparison to Observational Data

To ensure that ERA5 reanalysis data successfully capture the near-coast warming associated with the passage of western group TCs, daily average temperatures from NWS weather stations in the South Coast Drainage Basin region of California were also calculated for the days around TC occurrence. Figure 7 shows the temperature anomalies associated with TC occurrence from both ERA5 and NWS station data for the 24 western group TCs.

Figure 3. Composites for the 24 storms in the western group (left) and the 18 storms in the eastern group (right). (a) and (b) Storm tracks of the tropical cyclones (TCs) included in the analysis, with Hurricane Hilary highlighted. TCs that entered the red boxes shown were included in the composite analysis. (c) (d) Composites of 24-hr-averaged 500 hPa geopotential height anomalies and values. (e) and (f) Composites of 24-hr-averaged 2 m temperature anomalies and 850 hPa wind anomalies. (g) and (h) Composites of 5-day accumulated precipitation. The mean location of the TCs at their first timestep after they reach 29°N is shown as the black dots in panels (c)–(h), with the ellipse showing the area within two standard deviations.

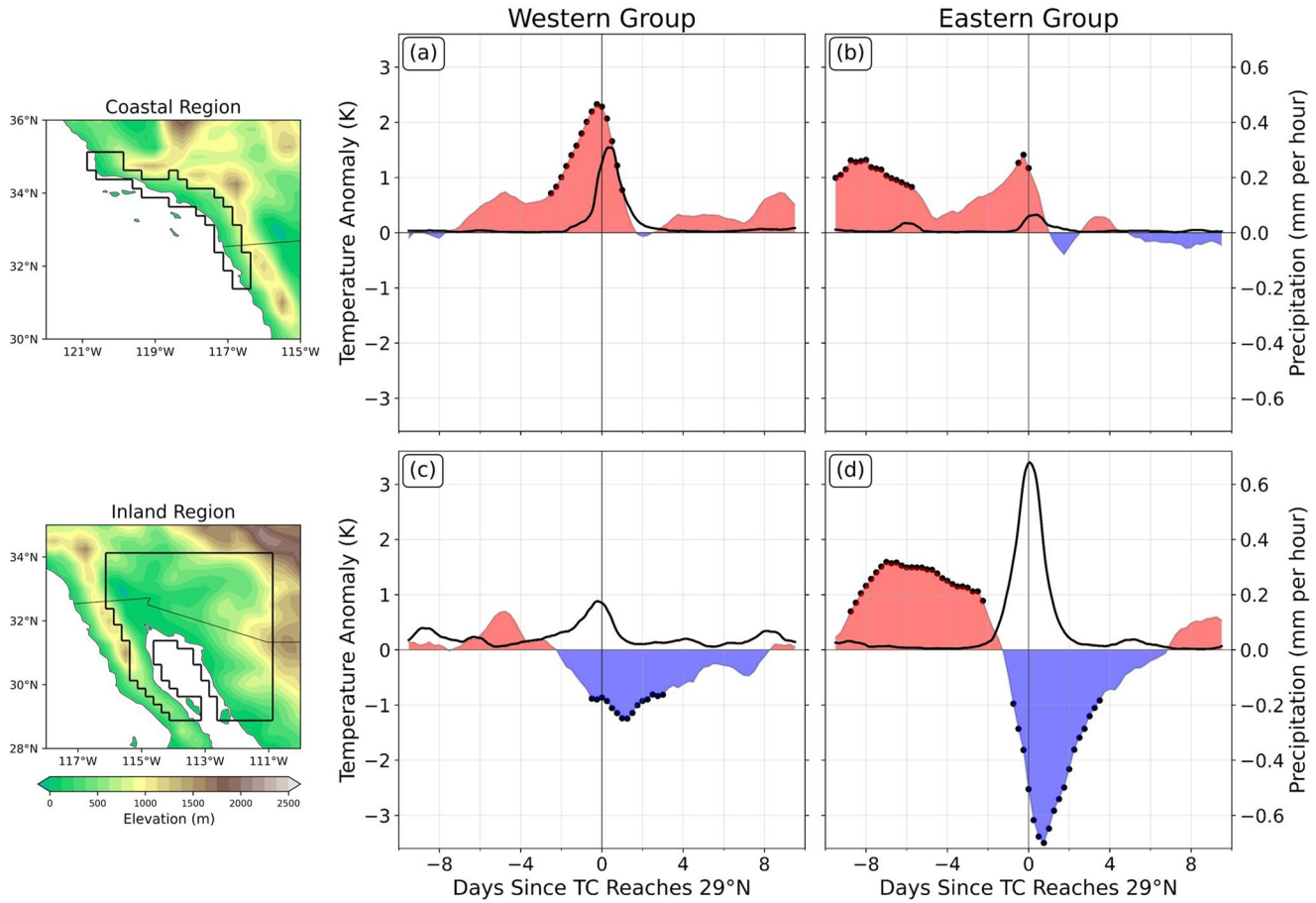

Figure 4. Composite timeseries of 2 m temperature and precipitation response to tropical cyclone (TC) events. (a) Response in coastal region for western group TCs. (b) Response in coastal region for eastern group TCs. (c) Response in inland region for western group TCs. (d) Response in inland region for eastern group TCs. Temperature anomalies are shown with red and blue shading, with black dots indicating where values are significant at 95%. Precipitation rates are shown as a solid black line. Both temperature and precipitation are shown as running means over a 24-hr period to remove diurnal variations.

There is good agreement between the two data sets, with station data showing warm anomalies that are similar spatially, temporally, and in magnitude to reanalysis data. This suggests that ERA5 is capturing the temperature response well and that our previous conclusions are valid.

There are some differences between the observed temperatures and the reanalysis; for example, temperature anomalies for stations around Los Angeles and those nearest the coast are slightly higher than in reanalysis for the day of TC occurrence and the day after. There is also more variation between neighboring stations in areas experiencing cold anomalies, particularly the day after TC occurrence. However, it is not surprising that data from an individual station can vary more and show higher temperatures anomalies than reanalysis which is averaged over a grid cell. Topography and proximity to the ocean is crucial to the observed TC-induced warming pattern and influences each station slightly differently. Furthermore, temperature data are not available for all TCs at all stations, which accounts for some of the difference between reanalysis and weather stations.

4. Discussions and Conclusions

Although rare, TCs do impact the SW US, bringing substantial precipitation and modulating temperatures regionally for over a week. Notable warming occurs in the populated coastal region of Southern California and Baja California preceding many of these TCs, particularly western group TCs that track offshore, with high temperatures driven by downslope winds, warm air advection, and a suppression of coastal upwelling. Inland,

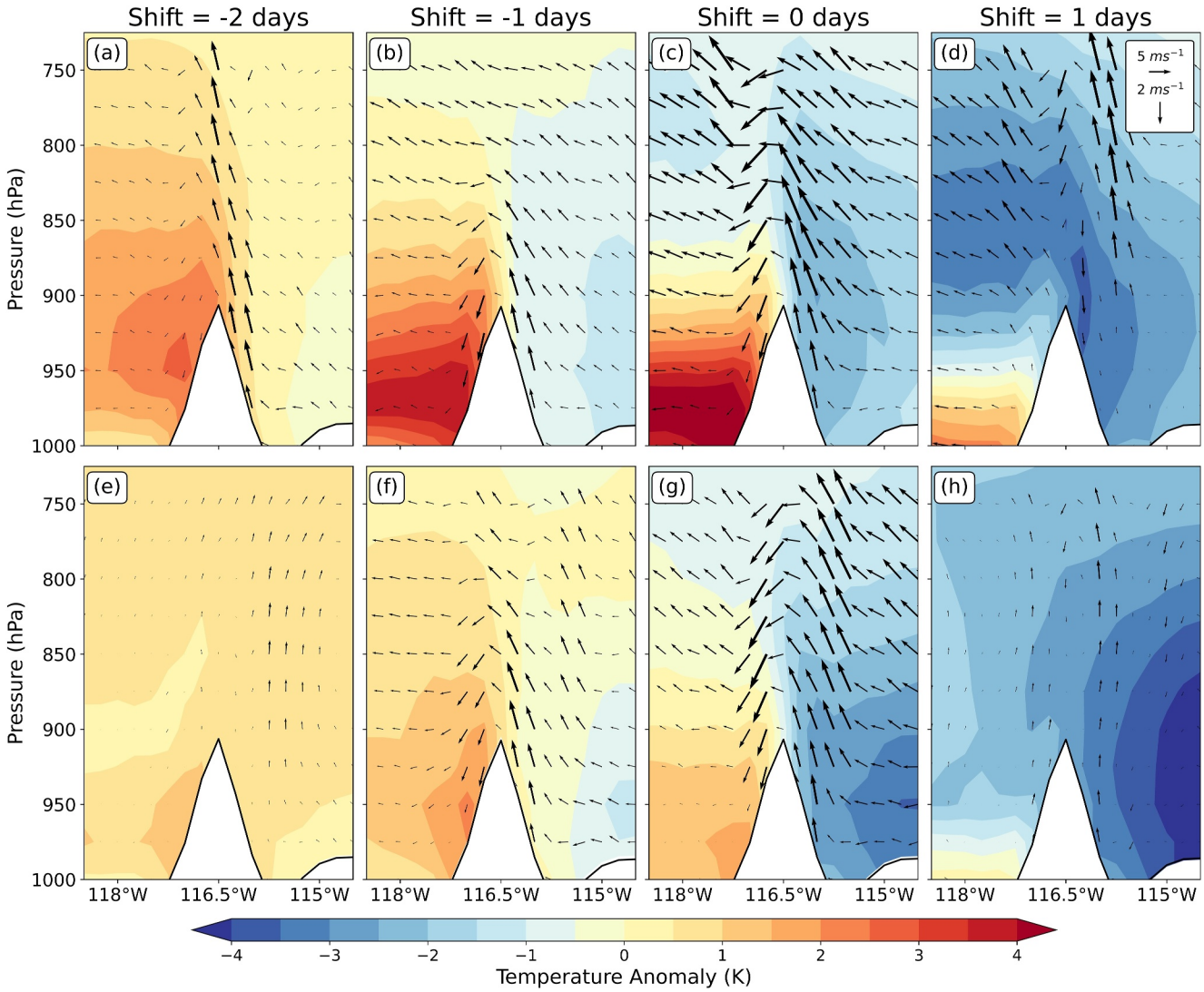

Figure 5. Vertical profiles of temperature and wind anomalies along a transect at 33°N, for the days prior to, during, and after tropical cyclones (TCs) reach 29°N. (a)–(d) show composites of western group TCs and (e)–(h) show eastern group TCs. The topography along this transect is shown in white. Note the different scale for vertical and zonal winds.

significant precipitation and evaporative cooling occurs as TCs pass, with temperatures falling almost 5°C during eastern group TCs.

The composite analysis presented in Figures 3 and 4 shows robust results; however, there can be large variations between individual storms. For example, Hilary in 2023 brought far more precipitation to the coastal region and cooled the inland region significantly more than other western group TCs. Background conditions also modulate the observed temperature response. For example, larger-scale heatwaves can occur at the same time as TCs, as observed prior to TC Kay in 2022 (Pratt, 2022), and SSTs can also be significantly different from the climatological mean (SSTs were much cooler than average during TC Hilda in 1991). Another issue with the composite method is that TCs do not reach 29°N at the same longitude, so there is a smearing effect that can distort the patterns of geopotential height anomalies. Although a TC-centered coordinate system (e.g., Hart et al., 2007) can remove this effect and produce clearer geopotential height composites, we choose not to use this method as it would obscure the influence of topography on local temperature and precipitation.

Although impacts from TC in the SW US are uncommon in the current climate, there are several factors that could increase this risk in the future. First, recent studies have suggested that climate change is causing a poleward shift

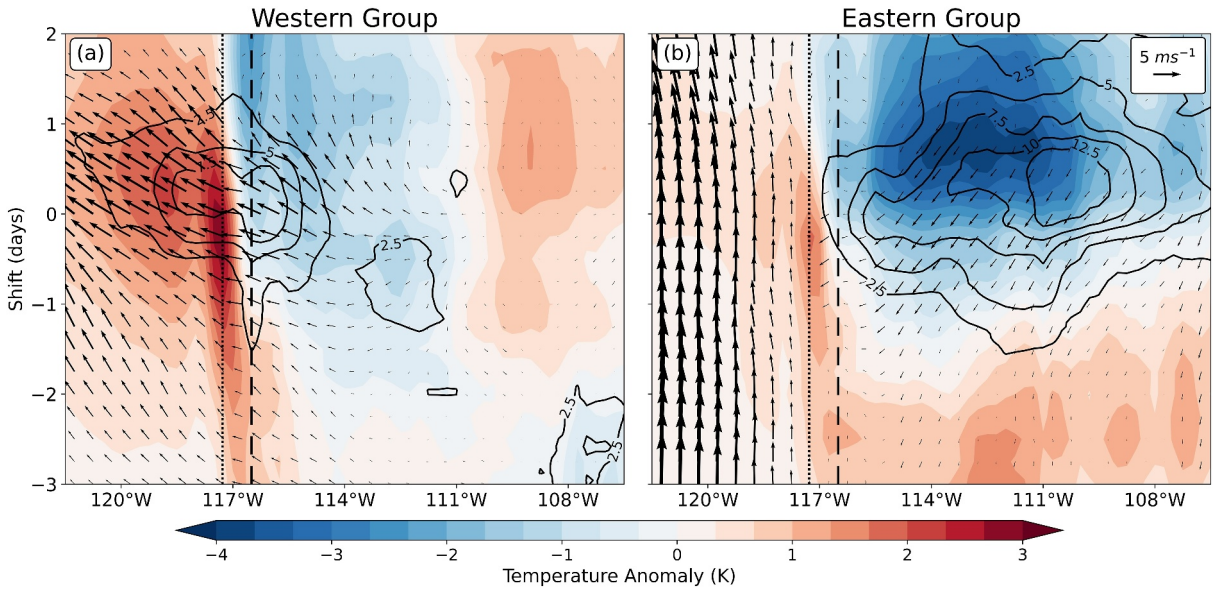

Figure 6. Temperature response to tropical cyclones (TCs) along a transect at 33°N. Hovmöller diagrams of 2 m temperature anomalies (colors), 850 hPa wind anomalies (arrows), and precipitation (contours) at 33°N for (a) western and (b) eastern group TCs. The precipitation values are averaged between 32° and 34°N, with contours shown in increments of 2.5 mm per day. The dashed black line shows the location of the peak of the peninsular mountain range, and the dotted black line shows the longitude of the coast at 33°N.

of TCs (X. Feng et al., 2021; Studholme et al., 2022) which, in combination with the documented westward shift in NEP TC tracks, could allow these systems to make landfall further north (S. Wang & Toumi, 2021). In particular, Hadley Cell expansion is expected to push subtropical highs polewards, which would likely reduce the high-pressure barrier that typically blocks TCs from approaching the SW US (Schmidt & Grise, 2017; Sharmila & Walsh, 2018). Additionally, as SSTs rise with climate change, TCs may weaken less quickly as they approach California. Finally, as the climate warms, rainfall rates associated with TCs are expected to increase (Guzman & Jiang, 2021). Along with sea-level rise, this is likely to increase the risk of flooding from TCs in the SW US. These factors are somewhat complicated by a projected decrease in overall TC counts; however, models suggest that the frequency of high-intensity TCs will increase (Knutson et al., 2010; Walsh et al., 2016).

With such a small sample size of extreme north-reaching TCs, it is hard to make robust conclusions on how the frequency of TCs that impact the SW US will change. From a preliminary analysis of TC counts, we find that although there is a positive trend in the annual frequency of NEP TCs from 1959 to 2023, there have been no significant trends in the number of TCs reaching 29°N, their maximum latitude, or the percentage of NEP TCs that occur late in the season when conditions are more favorable. Climate models can be used to generate large numbers of synthetic north-reaching TCs; however, it is difficult to generate realistic TC tracks for these fringe cases (Bell et al., 2019; Ishii & Mori, 2020). Given that there are still large uncertainties in how climate change will affect TCs on a global scale (Camargo et al., 2023), quantifying how the frequency and tracks of north-reaching TCs in the NEP may change in the future would be very challenging, and requires more detailed investigation than the brief discussion presented here.

Future studies could expand on our results by investigating societal and environmental impacts of TC-driven high temperatures and extreme rainfall in the SW US region. There is limited research on the vulnerability of local populations to TCs in the NEP (Dominguez et al., 2021; Marín-Monroy et al., 2020), and despite the rarity of TCs approaching the SW US, they are a hazard that could cause significant damage (Chenoweth & Landsea, 2004). Landfalling TCs can also impact coastal ecosystems (Feehan et al., 2024), and the anomalously warm SSTs observed as TCs approach the SW US could harm marine life (Smith et al., 2023), both of which may worsen as the oceans warm. There is still limited understanding of what a worst-case TC event for Southern California would look like, and climate change may further enhance the risk for this region (Bloemendaal et al., 2022).

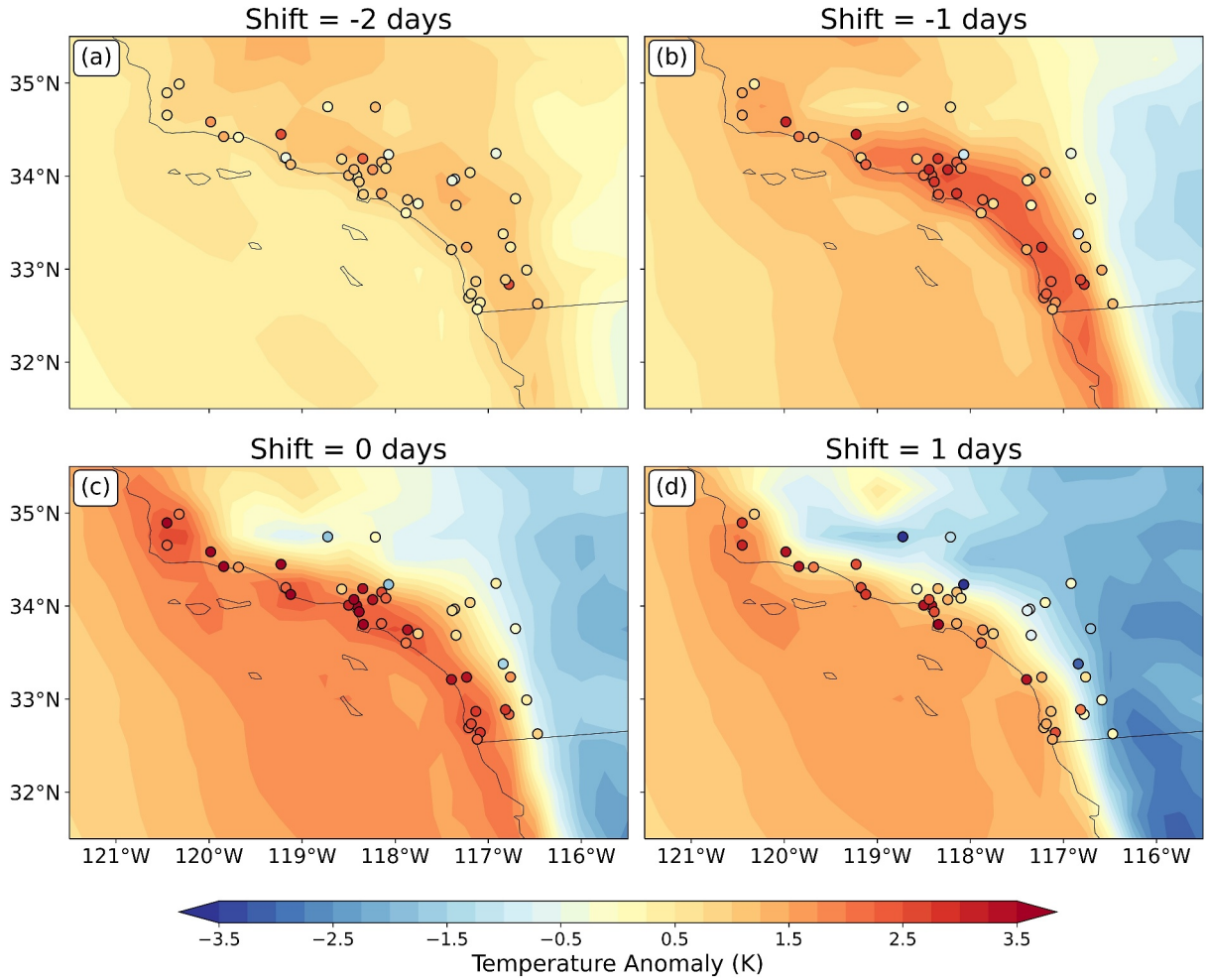

Figure 7. (a)–(b) Comparison of the temperature response to western group tropical cyclones (TCs) in the coastal region between reanalysis and observational data for the days preceding, (c) during and (d) after TCs reach 29°N. Filled contours show the daily average temperature anomalies derived from ERA5 reanalysis data, and filled circles show the daily average temperature anomalies at an individual NWS weather station. Data are not available for all TCs at all stations, so a station is only shown if there are data during at least 15 (70%) TCs, as noted in Table S3 in Supporting Information S1.

Data Availability Statement

All ERA5 data (Hersbach et al., 2020) used in this study are available to download from the ECMWF Climate Data Store at: https://cds.climate.copernicus.eu/. TC track data from 1959 to 2022 are available from the NHC HURDAT2 database (Landsea & Franklin, 2013), available at: https://www.nhc.noaa.gov/data/. Data for the track of Hurricane Hilary in 2023 were taken from the NHC's Tropical Cyclone Report on Hurricane Hilary (Reinhart, 2024), available at: https://www.nhc.noaa.gov/data/tcr/EP092023_Hilary.pdf. Figures were made with Matplotlib version 3.2.2 (Caswell et al., 2020; Hunter, 2007) available under the Matplotlib license at https://matplotlib.org/.

Acknowledgments
This study is supported by the National Science Foundation (AGS-2105654).

References

Bell, S. S., Chand, S. S., Tory, K. J., Turville, C., & Ye, H. (2019). Eastern North Pacific tropical cyclone activity in historical and future CMIP5 experiments: Assessment with a model-independent tracking scheme. *Climate Dynamics*, *53*(7), 4841–4855. https://doi.org/10.1007/s00382-019-04830-0

Blake, E. S., Rappaport, E. N., & Landsea, C. W. (2007). *The deadliest, costliest, and more intense United States tropical cyclones from 1851 to 2006 (and other frequently requested hurricane facts)*, *NOAA Technical Memorandum NWS TPC-5* (p. 43). U.S. Department of Commerce. Retrieved from https://www.nhc.noaa.gov/pdf/NWS-TPC-5.pdf

Bloemendaal, N., de Moel, H., Martinez, A. B., Muis, S., Haigh, I. D., van der Wiel, K., et al. (2022). A globally consistent local-scale assessment of future tropical cyclone risk. *Science Advances*, *8*(17), eabm8438. https://doi.org/10.1126/sciadv.abm8438

Camargo, S. J., Murakami, H., Bloemendaal, N., Chand, S. S., Deshpande, M. S., Dominguez-Sarmiento, C., et al. (2023). An update on the influence of natural climate variability and anthropogenic climate change on tropical cyclones. *Tropical Cyclone Research and Review*, *12*(3), 216–239. https://doi.org/10.1016/j.tcrr.2023.10.001

Camargo, S. J., Robertson, A. W., Gaffney, S. J., Smyth, P., & Ghil, M. (2007). Cluster analysis of typhoon tracks. Part I: General properties. *Journal of Climate*, *20*(14), 3635–3653. https://doi.org/10.1175/JCLI4188.1

Caron, L.-P., Boudreault, M., & Camargo, S. J. (2015). On the variability and predictability of eastern Pacific tropical cyclone activity. *Journal of Climate*, *28*(24), 9678–9696. https://doi.org/10.1175/JCLI-D-15-0377.1

Cassidy, E. (2023). *Hilary Soaks the Southwest* [Web Article]. NASA Earth Observatory. Retrieved from https://earthobservatory.nasa.gov/images/151733/hilary-soaks-the-southwest

Caswell, T. A., Droettboom, M., Lee, A., Hunter, J., Andrade, E. S. D., Firing, E., et al. (2020). Matplotlib v3.3.2 [Software]. *Zenodo*. https://doi.org/10.5281/zenodo.4030140

Chenoweth, M., & Landsea, C. (2004). The San Diego Hurricane of 2 October 1858. *Bulletin of the American Meteorological Society*, *85*(11), 1689–1698. https://doi.org/10.1175/BAMS-85-11-1689

Corbosiero, K. L., Dickinson, M. J., & Bosart, L. F. (2009). The contribution of eastern North Pacific tropical cyclones to the rainfall climatology of the southwest United States. *Monthly Weather Review*, *137*(8), 2415–2435. https://doi.org/10.1175/2009MWR2768.1

Doermann, L. (2023). *Heat Dome Descends on Central U.S.* [Web Article]. NASA Earth Observatory. Retrieved from https://earthobservatory.nasa.gov/images/151751/heat-dome-descends-on-central-us

Dominguez, C., Jaramillo, A., & Cuéllar, P. (2021). Are the socioeconomic impacts associated with tropical cyclones in Mexico exacerbated by local vulnerability and ENSO conditions? *International Journal of Climatology*, *41*(S1), E3307–E3324. https://doi.org/10.1002/joc.6927

Du, R., Zhang, G., & Huang, B. (2023). Observed surface wind field structure of severe tropical cyclones and associated precipitation. *Remote Sensing*, *15*, 11. https://doi.org/10.3390/rs15112808

Evans, C., Wood, K. M., Aberson, S. D., Archambault, H. M., Milrad, S. M., Bosart, L. F., et al. (2017). The extratropical transition of tropical cyclones. Part I: Cyclone evolution and direct impacts. *Monthly Weather Review*, *145*(11), 4317–4344. https://doi.org/10.1175/MWR-D-17-0027.1

Farfán, L. M., & Zehnder, J. A. (2001). An analysis of the landfall of Hurricane Nora (1997). *Monthly Weather Review*, *129*(8), 2073–2088. https://doi.org/10.1175/1520-0493(2001)129<2073:AAOTLO>2.0.CO;2

Feehan, C. J., Filbee-Dexter, K., Thomsen, M. S., Wernberg, T., & Miles, T. (2024). Ecosystem damage by increasing tropical cyclones. *Communications Earth & Environment*, *5*(1), 674. https://doi.org/10.1038/s43247-024-01853-2

Feng, K., Ouyang, M., & Lin, N. (2022). Tropical cyclone-blackout-heatwave compound hazard resilience in a changing climate. *Nature Communications*, *13*(1), 4421. https://doi.org/10.1038/s41467-022-32018-4

Feng, X., Klingaman, N. P., & Hodges, K. I. (2021). Poleward migration of western North Pacific tropical cyclones related to changes in cyclone seasonality. *Nature Communications*, *12*(1), 6210. https://doi.org/10.1038/s41467-021-26369-7

Fors, J. R. (1977). *Tropical Storm Kathleen*, *NOAA Technical Memorandum NWS WR-114* (p. 29). U.S. Department of Commerce. Retrieved from https://www.weather.gov/media/wrh/online_publications/TMs/TM-114.pdf

Gaffney, S. J. (2004). *Probabilistic curve -aligned clustering and prediction with regression mixture models* [Ph.D. Thesis]. Department of Computer Science, University of California.

Gershunov, A., Guzman Morales, J., Hatchett, B., Guirguis, K., Aguilera, R., Shulgina, T., et al. (2021). Hot and cold flavors of southern California's Santa Ana winds: Their causes, trends, and links with wildfire. *Climate Dynamics*, *57*(7), 2233–2248. https://doi.org/10.1007/s00382-021-05802-z

Gray, W. M. (1968). Global view of the origin of tropical disturbances and storms. *Monthly Weather Review*, *96*(10), 669–700. https://doi.org/10.1175/1520-0493(1968)096<0669:GVOTOO>2.0.CO;2

Gutzler, D. S., Wood, K. M., Ritchie, E. A., Douglas, A. V., & Lewis, M. D. (2013). Interannual variability of tropical cyclone activity along the Pacific coast of North America. *Atmósfera*, *26*(2), 149–162. https://doi.org/10.1016/S0187-6236(13)71069-5

Guzman, O., & Jiang, H. (2021). Global increase in tropical cyclone rain rate. *Nature Communications*, *12*(1), 5344. https://doi.org/10.1038/s41467-021-25685-2

Hanley, D. E., Bourassa, M. A., O'Brien, J. J., Smith, S. R., & Spade, E. R. (2003). A quantitative evaluation of ENSO indices. *Journal of Climate*, *16*(8), 1249–1258. https://doi.org/10.1175/1520-0442(2003)16<1249:AQEOEI>2.0.CO;2

Hart, R. E., Maue, R. N., & Watson, M. C. (2007). Estimating local memory of tropical cyclones through MPI anomaly evolution. *Monthly Weather Review*, *135*(12), 3990–4005. https://doi.org/10.1175/2007MWR2038.1

Hersbach, H., Bell, B., Berrisford, P., Hirahara, S., Horányi, A., Muñoz-Sabater, J., et al. (2020). The ERA5 global reanalysis. *Quarterly Journal of the Royal Meteorological Society*, *146*(730), 1999–2049. https://doi.org/10.1002/qj.3803

Higgins, R. W., & Shi, W. (2005). Relationships between Gulf of California moisture surges and tropical cyclones in the eastern Pacific basin. *Journal of Climate*, *18*(22), 4601–4620. https://doi.org/10.1175/JCLI3551.1

Hunter, J. D. (2007). Matplotlib: A 2D graphics environment. *Computing in Science & Engineering*, *9*(3), 90–95. https://doi.org/10.1109/MCSE.2007.55

Huyer, A. (1983). Coastal upwelling in the California current system. *Progress in Oceanography*, *12*(3), 259–284. https://doi.org/10.1016/0079-6611(83)90010-1

Ishii, M., & Mori, N. (2020). d4PDF: Large-ensemble and high-resolution climate simulations for global warming risk assessment. *Progress in Earth and Planetary Science*, *7*(1), 58. https://doi.org/10.1186/s40645-020-00367-7

Knutson, T. R., McBride, J. L., Chan, J., Emanuel, K., Holland, G., Landsea, C., et al. (2010). Tropical cyclones and climate change. *Nature Geoscience*, *3*(3), 157–163. https://doi.org/10.1038/ngeo779

Landsea, C. W., & Franklin, J. L. (2013). Atlantic hurricane database uncertainty and presentation of a new database format. *Monthly Weather Review*, *141*(10), 3576–3592. https://doi.org/10.1175/MWR-D-12-00254.1

Lawrence, M. B. (1999). Eastern North Pacific hurricane season of 1997. *Monthly Weather Review*, *127*(10), 2440–2454. https://doi.org/10.1175/1520-0493(1999)127<2440:ENPHSO>2.0.CO;2

Lin, I.-I., Camargo, S. J., Patricola, C. M., Boucharel, J., Chand, S., Klotzbach, P., et al. (2020). ENSO and tropical cyclones. In *El Niño Southern Oscillation in a Changing Climate* (pp. 377–408). American Geophysical Union (AGU). https://doi.org/10.1002/9781119548164.ch17

Marín-Monroy, E. A., Hernández-Trejo, V., Romero-Vadillo, E., & Ivanova-Boncheva, A. (2020). Vulnerability and risk factors due to tropical cyclones in coastal cities of Baja California Sur, Mexico. *Climate*, *8*(12), 144. https://doi.org/10.3390/cli8120144

Matthews, T., Wilby, R. L., & Murphy, C. (2019). An emerging tropical cyclone–deadly heat compound hazard. *Nature Climate Change*, *9*(8), 602–606. https://doi.org/10.1038/s41558-019-0525-6

Milet, M., Samuel, M., Hoshiko, S., Radhakrishna, R., & Aragón, T. (2023). *Excess mortality during the September 2022 heat wave in California* [Report]. California Department of Public Health, Office of Health Equity. Retrieved from https://www.cdph.ca.gov/Programs/OHE/CDPH%20Document%20Library/Climate-Health-Equity/CDPH-2022-Heat-Wave-Excess-Mortality-Report.pdf

Murakami, H., Vecchi, G. A., Delworth, T. L., Wittenberg, A. T., Underwood, S., Gudgel, R., et al. (2017). Dominant role of subtropical Pacific warming in extreme eastern Pacific hurricane seasons: 2015 and the future. *Journal of Climate*, *30*(1), 243–264. https://doi.org/10.1175/JCLI-D-16-0424.1

National Hurricane Center. (2023). *Hurricane Hilary Discussion Number 9* [Web Article]. NOAA, U.S. Department of Commerce. Retrieved from https://www.nhc.noaa.gov/archive/2023/ep09/ep092023.discus.009.shtml?

Pratt, S. E. (2022). *A long-lasting western heatwave* [Web Article]. NASA Earth Observatory. Retrieved from https://earthobservatory.nasa.gov/images/150318/a-long-lasting-western-heatwave

Reinhart, B. J. (2024). *Tropical cyclone report: Hurricane Hilary* [Report]. NOAA, U.S. Department of Commerce. Retrieved from https://www.nhc.noaa.gov/data/tcr/EP092023_Hilary.pdf

Ritchie, E. A., Wood, K. M., Gutzler, D. S., & White, S. R. (2011). The influence of eastern Pacific tropical cyclone remnants on the southwestern United States. *Monthly Weather Review*, *139*(1), 192–210. https://doi.org/10.1175/2010MWR3389.1

Rogers, P. J., & Johnson, R. H. (2007). Analysis of the 13–14 July Gulf Surge Event during the 2004 North American Monsoon Experiment. *Monthly Weather Review*, *135*(9), 3098–3117. https://doi.org/10.1175/MWR3450.1

Schmidt, D. F., & Grise, K. M. (2017). The response of local precipitation and sea level pressure to Hadley cell expansion. *Geophysical Research Letters*, *44*(20), 10573–10582. https://doi.org/10.1002/2017GL075380

Sharmila, S., & Walsh, K. J. E. (2018). Recent poleward shift of tropical cyclone formation linked to Hadley cell expansion. *Nature Climate Change*, *8*(8), 730–736. https://doi.org/10.1038/s41558-018-0227-5

Smith, K. E., Burrows, M. T., Hobday, A. J., King, N. G., Moore, P. J., Sen Gupta, A., et al. (2023). Biological impacts of marine heatwaves. *Annual Review of Marine Science*, *15*(1), 119–145. https://doi.org/10.1146/annurev-marine-032122-121437

Smith, W. (1986). *The effects of Eastern North Pacific tropical cyclones on the Southwestern United States*, *NOAA Technical Memorandum NWS WR-197* (p. 229). U.S. Department of Commerce. Retrieved from https://repository.library.noaa.gov/view/noaa/7105

Steen, M., Castellano, C., Roj, S., Iñiguez, J., Cordeira, J., & Kalansky, J. (2023). *CW3E Event Summary: Hurricane Hilary 20-21 August 2023* [Web Article]. Center for Western Weather and Water Extremes. Retrieved from https://cw3e.ucsd.edu/cw3e-event-summary-hurricane-hilary-20-21-august-2023/

Student. (1908). The probable error of a mean. *Biometrika*, *6*(1), 1–25. https://doi.org/10.2307/2331554

Studholme, J., Fedorov, A. V., Gulev, S. K., Emanuel, K., & Hodges, K. (2022). Poleward expansion of tropical cyclone latitudes in warming climates. *Nature Geoscience*, *15*, 1–28. https://doi.org/10.1038/s41561-021-00859-1

U.S. Climate Resilience Toolkit. (2024). SC-ACIS—Applied Climate Information System Version 2 [Dataset]. *SC ACIS*. Retrieved from https://scacis.rcc-acis.org/

Walsh, K. J. E., McBride, J. L., Klotzbach, P. J., Balachandran, S., Camargo, S. J., Holland, G., et al. (2016). Tropical cyclones and climate change. *WIREs Climate Change*, *7*(1), 65–89. https://doi.org/10.1002/wcc.371

Wang, P., Yang, Y., Xue, D., Qu, Y., Tang, J., Leung, L. R., & Liao, H. (2023). Increasing compound hazards of tropical cyclones and heatwaves over southeastern coast of China under climate warming. *Journal of Climate*, *36*(7), 2243–2257. https://doi.org/10.1175/JCLI-D-22-0279.1

Wang, S., & Toumi, R. (2021). Recent migration of tropical cyclones toward coasts. *Science*, *371*(6528), 514–517. https://doi.org/10.1126/science.abb903

Wei, X., Li, K.-Y., Kilpatrick, T., Wang, M., & Xie, S.-P. (2021). Large-scale conditions for the record-setting Southern California marine heatwave of August 2018. *Geophysical Research Letters*, *48*(7), e2020GL091803. https://doi.org/10.1029/2020GL091803